J. Fluid Mech. (2004), *vol.* 521, *pp.* 191–215.
DOI: 10.1017/S0022112004001818 Printed in the United Kingdom

Energy cascade and spatial fluxes in wall turbulence

By N. MARATI, C. M. CASCIOLA AND R. PIVA

Dipartimento di Meccanica e Aeronautica, Università di Roma La Sapienza, Via Eudossiana 18, 00184 Roma, Italy

(Received 3 November 2003 and in revised form 4 August 2004)

Real turbulent flows are difficult to classify as either spatially homogeneous or isotropic. Nonetheless these idealizations allow the identification of certain universal features associated with the small-scale motions almost invariably observed in a variety of different conditions. The single most significant aspect is a flux of energy through the spectrum of inertial scales related to the phenomenology commonly referred to as the Richardson cascade. Inhomogeneity, inherently present in near-wall turbulence, generates additional energy fluxes of a different nature, corresponding to the spatial redistribution of turbulent kinetic energy. Traditionally the spatial flux is associated with a single-point observable, namely the turbulent kinetic energy density. The flux through the scales is instead classically related to two-point statistics, given in terms of an energy spectrum or, equivalently, in terms of the second-order moment of the velocity increments. In the present paper, starting from a suitably generalized form of the classical Kolmogorov equation, a scale-by-scale balance for the turbulent fluctuations is evaluated by examining in detail how the energy associated with a specific scale of motion – hereafter called the scale energy – is transferred through the spectrum of scales and, simultaneously, how the same scale of motion exchanges energy with a properly defined spatial flux. The analysis is applied to a data set taken from a direct numerical simulation (DNS) of a low-Reynolds-number turbulent channel flow. The detailed scale-by-scale balance is applied to the different regions of the flow in the various ranges of scales, to understand how – i.e. through which mechanisms, at which scales and in which regions of the flow domain – turbulent fluctuations are generated and sustained. A complete and formally precise description of the dynamics of turbulence in the different regions of the channel flow is presented, providing rigorous support for previously proposed conceptual models.

1. Introduction

Wall-bounded turbulence is characterized by several processes which may be thought of as belonging to two different classes: phenomena which occur in physical space and phenomena which take place in the space of scales. A typical example of the former is the spatial flux of turbulent kinetic energy. A concept related to the latter is the energy transfer among scales due to the coupling between modes, or, in more general terms, between eddies of different size.

Wall-bounded flows present well-characterized regions where the different contributions to the balance of turbulent kinetic energy, namely viscous, inertial and production terms, play different roles. In particular, a turbulent channel flow is classically sub-divided into a viscosity-dominated sublayer, a buffer layer where

production of turbulent kinetic energy and turbulence intensity is the largest, a logarithmic layer, with production in equilibrium with dissipation, and finally a core region where turbulence is energized by the spatial flux of turbulent kinetic energy generated within the buffer layer, see the monograph by Townsend (1956), the comprehensive review in Pope (2000) and references cited therein. This classical picture, common to different wall-bounded flows (see e.g. the experimental analysis by Eckelmann (1974) for the channel flow and by Klebanoff (1954) for the boundary layer) has been made even clearer in recent times through the analysis of the data sets generated by highly accurate numerical simulations. Direct numerical simulations (DNS, see e.g. Kim, Moin & Moser 1987; Moser, Kim & Mansour 1999) show the role of inhomogeneity in connection with the self-sustaining capability of wall-bounded turbulence. In this context, DNS has been used to construct so-called 'unphysical experiments', Jimenez & Pinelli (1999), with the aim of addressing specific mechanisms of turbulence regeneration (see e.g. Hamilton, Kim & Waleffe 1995). Globally, these results, obtained by addressing the flow dynamics in physical space, make clear that production by mean shear, flux of turbulent kinetic energy and dissipation are the principal ingredients in understanding the dynamics of wall-bounded flows.

The description in physical space alone is however insufficient to capture the real dynamics of wall-bounded turbulence, and traditionally it is complemented by a parallel view based on the decomposition of the field into a hierarchy of scales of motion. In fact, according to the classical prediction of Kolmogorov (1941), every turbulent flow at sufficiently large Reynolds number is expected to approach a universal state at small scales, see also Monin & Yaglom (1975). There is much experimental evidence that this is true in the log-layer, where the longitudinal energy spectrum is found to scale for a significant range like the power $-5/3$ of the wavenumber, $k^{-5/3}$, see e.g. the experiments of Saddoughi & Veeravalli (1994) in a large-Reynolds-number boundary layer and the compilation of a huge amount of data of different origin reported therein. The review paper by Gad-el-Hak & Bandyopadhyay (1994) is also worth mentioning in this context for the assessment of finite Reynolds number effects. Actually, the longitudinal spectrum in the log-layer exhibits several distinct ranges: apart from a dissipative range and a classical inertial range, at larger separations – namely for wavenumbers smaller than the reciprocal of the distance from the wall – a distinct range with scaling behaviour proportional to k^{-1} emerges as discussed in the paper by Perry, Henbest & Chong (1986); see also Nikora (1999) for theoretical arguments on the subject. In this so-called production range the turbulent fluctuations are generated by the direct action of the local shear. The entire turbulence statistics is strongly affected by the shear and the picture is substantially different from the classical description in terms of the Richardson cascade, see e.g. Frisch (1995) for a general discussion of the energy cascade issue in homogeneous isotropic turbulence, to the extent that even the level of intermittency is enhanced as shown by the scaling properties of the structure functions of the turbulent field, see the analysis of DNS data in Toschi *et al.* (1999) and Benzi *et al.* (1999) and the experimental results of Ruiz-Chavarria *et al.* (2000) and Jacob, Olivieri & Casciola (2002).

The two complementary approaches just outlined above are in a sense mutually exclusive, since addressing one precludes the other automatically. In this respect, a more general approach is clearly necessary to describe the scale-dependent dynamics in the presence of the spatial fluxes induced by the inhomogeneity. Recently an equation with these characteristics has been derived by Hill (2002) as an evolution equation for the second-order moment of the velocity increment between two locations, namely

the second-order structure function, as a function of separation and position of the mid-point. The procedure to derive the equation is discussed in detail and is sufficiently general to allow its extension to higher orders as discussed by Hill & Borotav (2001). By a different approach these results confirmed those derived from the evolution equation for the generating function of the probability distribution of the velocity increments by Yakhot (2001). He showed how the hierarchy of equations for velocity structure functions is not closed due to terms arising from the statistics of the dissipation field and to pressure–velocity correlations. Suitable closures are introduced as a necessary step to reach quantitative predictions on the scaling exponents of the structure functions. The subject has been re-considered by Kurien & Sreenivasan (2001) who gave a further contribution by checking both assumptions and predictions of the theory against experimental data.

In this context, the focus of the present paper is on the equation for the second-order structure function. Interpreted in terms of fluctuation velocity, this generalized Kolmogorov equation reduces to the classical form when homogeneous isotropic conditions are approached, while under uniform shear it reproduces the equation used for the scale-by-scale budget in homogeneous shear flow, Casciola *et al.* (2003) (see also Hinze 1959 and Oberlack 2001 for the derivation of closely related equations). By this kind of approach it has recently been shown that the production range and classical inertial range of shear-dominated flows possess several universal features. For instance, the scaling laws for the longitudinal velocity increments in the homogeneous shear flow, Gualtieri *et al.* (2002), are reproduced with exactly the same characteristics in a zero-pressure-gradient boundary layer, Casciola *et al.* (2002).

Up to now the great potential of a general equation for the second-order structure function has never been fully exploited in an analysis of inhomogeneous turbulent fields. An exception is the paper of Danaila *et al.* (2000) where hot-wire anemometry data taken in the core of a turbulent channel flow are analysed with the main motivation of providing improved estimates of the dissipation rate in slightly inhomogeneous conditions, see also Lindborg (1999) on a related topic. From the experimental point of view, however, a number of assumptions are necessary to evaluate the different terms of the equation from hot-wire measurements.

In the present paper the generalized Kolmogorov equation is used in its full form to reveal the dynamics of the turbulent fluctuations at different scales in the different regions of a turbulent channel flow described through a DNS at a friction Reynolds number of 180. The main purpose is to assess the role of two fluxes of scale energy of essentially different nature: one, taking place in physical space, is generated by the inhomogeneity of the field; the other, occurring in the space of scales, constitutes the natural generalization of the energy transfer associated with the Richardson cascade. The detailed scale-by-scale balance, applied to the different regions in the various ranges of scales, allows us to understand through which mechanisms, at which scales and in which regions of the flow domain turbulent fluctuations are generated and sustained.

The material is organized as follows. After this Introduction, § 2 consists of a detailed description of the numerical data set and recalls the basic concepts in wall turbulence. Section 3 introduces the generalized Kolmogorov equation and some of its basic properties. Section 4 discusses the two kind of fluxes, in physical space and through the scales, respectively. In § 5 the detailed scale-by-scale balance in the different regions of the channel is discussed in detail while in the last section a summary of the main findings and some final remarks are made. An appendix is also included to assess the statistical quality of the data set used for the present analysis.

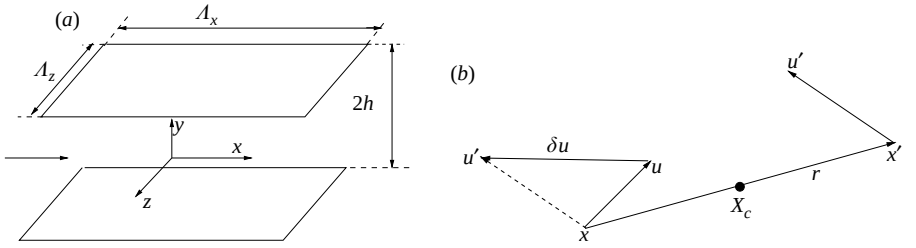

FIGURE 1. (*a*) Flow configuration and nomenclature for the channel flow. The flow is from left to right in the direction of the mean flow $U(y)$. The streamwise direction is $x \equiv x_1$. The wall-normal and the spanwise coordinates are $y \equiv x_2$ and $z \equiv x_3$, respectively. The corresponding fluctuation velocity components are denoted by $u \equiv u_1$, $v \equiv u_2$ and $w \equiv u_3$, respectively. (*b*) Sketch of the arrangement for two-point correlations. The velocities evaluated at $\boldsymbol{x}'$ ($\boldsymbol{u}'$) and at $\boldsymbol{x}$ ($\boldsymbol{u}$) are used to construct the increment $\delta\boldsymbol{u}$. The separation vector is $\boldsymbol{r}$, while $\boldsymbol{X}_c$ denotes the mid-point. In the channel flow, the typical two-point observable, say $\langle \delta u^2 \rangle$, is a function of the wall-normal coordinate of the mid-point $Y_c = \frac{1}{2}(y + y')$ and of the three components of the separation vector r_x, r_y and r_z.

2. Assessment of the data set

The simplest conditions in which to analyse the effect of inhomogeneity on the dynamics of the small scales of a turbulent flow are provided by the geometry of a channel between planar parallel walls, as sketched in figure 1(*a*). In this case turbulence is statistically invariant under translations in the streamwise x and the spanwise z directions, and time t, confining inhomogeneity only to the wall-normal direction y. Consistently, any statistical observable involving n_p spatial points, see figure 1(*b*) for the case $n_p = 2$, will depend only on a single y-coordinate and on $n_p - 1$ separation vectors in such a way that ergodicity can be exploited to perform ensemble averaging $\langle q \rangle$ of a given quantity q in terms of spatial averages in wall parallel planes (x, z) and in time.

In order to avoid the introduction of difficult to control simplifying assumptions, a large and detailed data-set is required to explore the spatial and temporal structure of the fluctuating field, given by the velocity components $u(x, y, z, t)$, $v(x, y, z, t)$, $w(x, y, z, t)$ and by the pressure field $p(x, y, z, t)$. These requirements suggest the use of results from a direct numerical simulation (DNS). The standard geometrical configuration consists of a portion of a channel infinite in the streamwise and spanwise directions. In this computational box with sides $(\Lambda_x, 2h, \Lambda_z)$, where h is the channel half-width and $-h \leqslant y \leqslant h$, periodic boundary condition are imposed in x and z, with standard impermeability and no-slip on the solid walls. A mean pressure gradient $\mathrm{d}\langle p \rangle / \mathrm{d}x$ is enforced to guarantee a prescribed mass flux M through the channel, associated with the mean flow $U(y)$.

Given obvious limitations on the available computational resources, only low-Reynolds-number flows can be treated by DNS, which, on the other hand, is by definition, the appropriate numerical tool to achieve a resolution up to the dissipation scales. For the simulation, we rely on a well-established highly accurate numerical formulation given by a spectral method exploiting Fourier–Chebyshev–Fourier expansions in terms of the wall-normal components of velocity and vorticity coupled with a mixed Crank–Nicholson/Runge–Kutta scheme for time advancement, Lundbladh, Henningson & Johansson (1992). The friction Reynolds number $Re_* = u_* h / \nu$, where ν is the kinematic viscosity and $u_* = \sqrt{\tau_0 / \rho}$ is the so-called friction velocity expressed in terms of the average shear stress τ_0 at the wall and

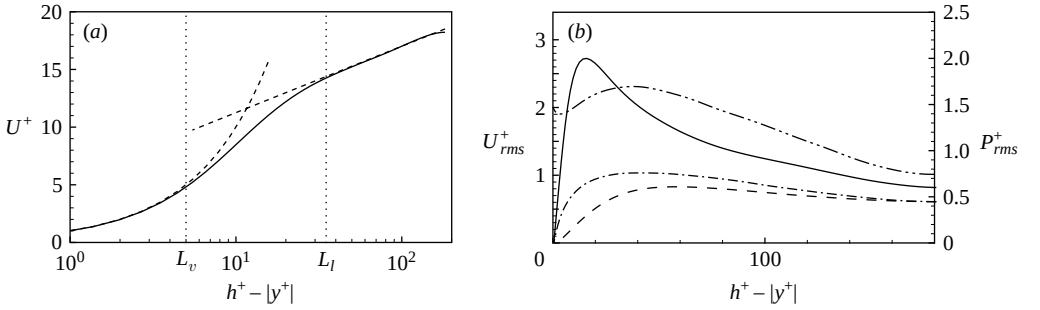

FIGURE 2. (*a*) Mean velocity profile U^+ in viscous units vs. distance from the wall $(h-|y|)^+$, solid line. The dashed lines denote the linear and the log-law with a Kármán constant $k=0.41$. Classically the near-wall region is subdivided into the viscous sublayer $0 \leqslant (h-|y|)^+ \leqslant L_v^+$, the buffer layer $L_v^+ \leqslant (h-|y|)^+ \leqslant L_l^+$ and the log-layer above L_l^+ extending up to the bulk region where the mean profile deviates from the log-law. Typically, for Newtonian turbulence, $L_v^+ \simeq 5$ and $L_v^+ \simeq 30$. (*b*) Fluctuation intensities vs. distance from the wall. Velocities u^+_{rms}(——), v^+_{rms}(— · —), w^+_{rms}(— —), and pressure p^+_{rms}(— ·· —).

the density ρ, is fixed to 180 to reproduce conditions well-explored in the literature (Kim *et al.* 1987). The corresponding bulk Reynolds number is $Re_b = u_b\, h/\nu = 2600$, where u_b is the velocity averaged through the channel section given by $M/(2\rho h)$. We select $4 \times 2 \times 2$ as the dimensions of the computational domain, which are close to a minimum channel configuration (Jimenez & Moin 1991), with the number of grid points equal to $256 \times 129 \times 128$. In order to accumulate the statistics required for a well-converged analysis of the scale-by-scale budget in inhomogeneous conditions, long runs with small time step are mandatory. Our principal run has been continued, after reaching a statistically steady state, for about $N = 2400$ large-eddy turnover times $T = h/U_{cl}$, where U_{cl} is the average velocity at the centreline; for the principal run considered here $U_{cl} = 0.8$, with a time step $\mathrm{D}t = 0.04$. About 300 statistically uncorrelated configurations of the channel were saved to disk to evaluate the pressure field by post-processing and finally performing the statistical analysis. The length of the simulation has a specific motivation. In the viscous sublayer the coherent structures – the so-called streaks – have a very long survival time, of order more than 500 inner time units (Kline *et al.* 1967). Since our computational domain is close to a minimal channel unit (Jimenez & Moin 1991) only a few streaks are present in each configuration (order of two or three – we checked the results against a shorter, less-resolved simulation in a larger computational domain, see the Appendix). Hence we cannot rely too strongly on spatial ergodicity. This implies that temporally uncorrelated configurations are needed to obtain reliable statistics, hence the length of the run.

Before describing the main achievements of the work, we briefly discuss the overall quality of the data-set with the twofold purpose of introducing notation and recalling some known results on the dynamics of the channel flow, as described by low-Reynolds-number simulations.

The mean velocity profile $U(y)$, normalized by the friction velocity, is shown in figure 2(*a*) in comparison with the expected linear behaviour $U^+ = U/u_* = (h-|y|)^+$ in the viscous sublayer, and the logarithmic law $U^+ = (1/k)\,\log(h-|y|)^+ + 5.5$ with Kármán constant of 0.4 (see e.g. Zagarola & Smits (1997) for a discussion of the scaling properties of the mean velocity profile in wall-bounded flows). The two dotted lines approximately define the boundary of the viscous sublayer, $(h-|y|)^+ = L_v^+$, and

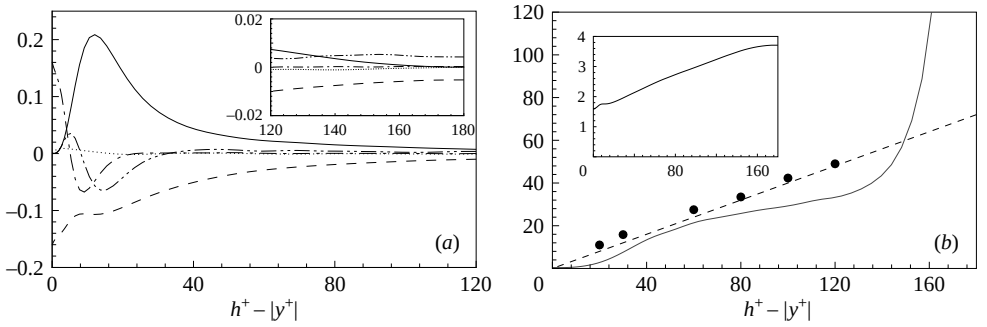

FIGURE 3. (*a*) Turbulent kinetic energy budget vs. distance from the wall $(h-|y|)^+$: production (——), viscous diffusion (— · —), pressure transport (· · ·), turbulent convection (— · · —), and dissipation (— —), see equation (2.1). The details of the central region are shown in the inset. (*b*) The solid line is $L_s = \sqrt{\epsilon/S^3}$ (in wall units) vs. distance from the wall. The dashed line corresponds to $k\,(h-|y|)^+$ and the circles denote the crossover scale ℓ_c^+ between the production and energy cascade term in viscous units, see equation (5.4). The inset is the Kolmogorov scale η^+ vs. distance from the wall.

the lower limit of the log-region, $(h-|y|)^+ = L_l^+$. As usual $(h-|y|)^+ = (h-|y|)u_*/\nu$ denotes the distance from the wall expressed in wall units, and a superscript + will in general imply a quantity made dimensionless with respect to u_*, ν and ρ. The reader may wish to return to figure 2 as a schematic visualization of the different regions of the flow which are discussed in the forthcoming sections of the paper.

The wall-normal distributions of turbulent intensities u_{rms}, v_{rms} and w_{rms}, normalized by the wall shear velocity, are shown in figure 2(*b*). The peak of u_{rms} is reached at $(h-|y|)^+ \simeq 15$, near the location of maximum kinetic energy production, see figure 3(*a*). The root-mean-square pressure fluctuation, normalized by $\rho {u_*}^2$, is shown by the dash-double dotted line, see Kim *et al.* (1987) for a comparison.

The different terms in the equation for the turbulent kinetic energy,

$$-\langle uv\rangle \frac{\mathrm{d}U}{\mathrm{d}y} - \frac{1}{2}\frac{\mathrm{d}}{\mathrm{d}y}\langle u_i u_i v\rangle + \frac{\nu}{2}\frac{\mathrm{d}^2\langle u_i u_i\rangle}{\mathrm{d}y^2} - \frac{1}{\rho}\frac{\mathrm{d}\langle pv\rangle}{\mathrm{d}y} - \langle\epsilon\rangle = 0, \tag{2.1}$$

namely production, turbulent convection, viscous diffusion, pressure transport and pseudo-dissipation $\epsilon = \nu\langle(\partial u_i/\partial x_j)(\partial u_i/\partial x_j)\rangle$, respectively, are reported in figure 3(*a*), where the inset shows the detailed behaviour of various terms in the core region of the flow to be addressed in § 4.

Introducing the definition of the overall flux of turbulent kinetic energy,

$$\phi(y) = \tfrac{1}{2}\langle u_i u_i v\rangle - \frac{\nu}{2}\frac{\mathrm{d}\langle u_i u_i\rangle}{\mathrm{d}y} + \frac{1}{\rho}\langle pv\rangle \tag{2.2}$$

equation (2.1) becomes

$$\frac{\mathrm{d}\phi(y)}{\mathrm{d}y} = \sigma(y), \tag{2.3}$$

where $\sigma(y) = \pi(y) - \langle\epsilon(y)\rangle$ is the net source at location y given as the difference between production $\pi = -\langle uv\rangle \mathrm{d}U/\mathrm{d}y$ and average dissipation. By integration of equation (2.3) from the wall to the current location $\bar{y}$, the flux $\phi(\bar{y})$ is interpreted as the amount of turbulent kinetic energy per unit time and area which leaves the layer $-h \leqslant y \leqslant \bar{y}$ to enter the region above.

Around the peak, π is substantially greater than $\langle\epsilon\rangle$ and there the turbulent energy flux contributes to the energy supply of regions both below and above. In the logarithmic region of large-Reynolds-number flows, instead, the production–dissipation ratio is nearly unity and the flux is almost constant. The energy carried by ϕ through this equilibrium layer is spent in sustaining the fluctuations in the bulk region of the flow. Despite the fact that the asymptotic equilibrium state has not been reached yet at the Reynolds number of the present simulation, the energy intercepted in the log-region is nonetheless a small fraction of the amount locally produced by the shear, leaving the gross features unchanged.

Figure 3(*b*) shows the shear scale $L_s = \sqrt{\epsilon/S^3}$, where $S = \mathrm{d}U/\mathrm{d}y$, which at large Reynolds number, in the log-region, is expected to behave linearly with the wall distance, $L_s \simeq k(h - |y|)$. The symbols denote the cross-over scale between the production and the transport term which contributes to the energy cascade as will be discussed in § 5. The Kolmogorov scale $\eta = (\nu^3/\epsilon)^{1/4}$ in wall units is shown in the inset to evaluate the resolution of the simulation, namely $\Delta x^+ = 2.8$, $\Delta z^+ = 2.78$ and Δy^+ varying from 0.05 to 4.4 from the wall to the channel centreline, which is largely sufficient to achieve a well-resolved DNS.

3. The generalized Kolmogorov equation

The turbulent kinetic energy balance (2.1) alone is insufficient to satisfactorily describe the dynamics of a turbulent flow. Turbulence in wall-bounded flows is characterized by several interacting processes, such as energy production, spatial redistribution, energy cascade and dissipation. The relative importance of different phenomena may change significantly depending on the geometrical location (i.e. the distance from the wall) and the range of scales considered. A complete understanding of these interacting phenomena requires a detailed description of the processes occurring simultaneously in the geometric space and in the space of turbulent scales. One should be able to address the energy content of a given scale and evaluate its dependence on the spatial position. The proper quantity to consider is the so-called second-order structure function defined as $\langle\delta u^2\rangle$, where $\delta u^2 = \delta u_i \delta u_i$ and $\delta u_i = u_i(x_s + r_s) - u_i(x_s)$ denotes the fluctuating velocity increment. Loosely speaking, $\langle\delta u^2\rangle$ measures the amount of fluctuation energy at scale $r = \sqrt{r_s r_s}$ and therefore, following Danaila *et al.* (2000), it will be hereafter referred to as scale energy. From its definition, the scale energy depends on r – more precisely on the separation vector $r_i = x_i' - x_i$ – and on the location specified by the mid-point $X_{ci} = \frac{1}{2}(x_i' + x_i)$, see figure 1(*b*) for a sketch of the arrangement.

Figure 4(*a*) shows the isolines of the scale energy on the plane r_x, Y_c for $r_y = r_z = 0$, i.e. the function $\langle\delta u^2(r_x, 0, 0|Y_c)\rangle$, where $Y_c = \frac{1}{2}(y + y')$ is the wall-normal coordinate of the mid-point. Usually, structure functions are plotted as functions of separation, using the wall-normal position as a parameter. In our context, the present, slightly unconventional, representation in terms of isolines in the (r_x, Y_c)-plane has the advantage of combining, in a synthetic way, the description of the field in physical space (Y_c) and in the space of turbulent scales (r_x). The expected small-scale asymptotics of the scale energy, given by $\langle\delta u^2\rangle \simeq \langle(\partial u/\partial x)^2 + (\partial v/\partial x)^2 + (\partial w/\partial x)^2\rangle\, r_x^2$, is consistent with the behaviour near the Y_c-axis of the figure. The near-wall asympotics, i.e. for $|Y_c| \simeq h$, given by $\langle\delta u^2\rangle \simeq 2\langle\delta\tau_x^2 + \delta\tau_z^2\rangle\,(h - |Y_c|)^2/(\rho\nu)^2$, where $\langle\delta\tau_{x/z}^2\rangle$ denotes the mean-square fluctuation of the x/z-component of the instantaneous wall shear stress increment at the considered separation, is also apparent near the r_x-axis. For clarity, $\langle\delta u^2\rangle$ as a function of the wall-normal distance is also reported in

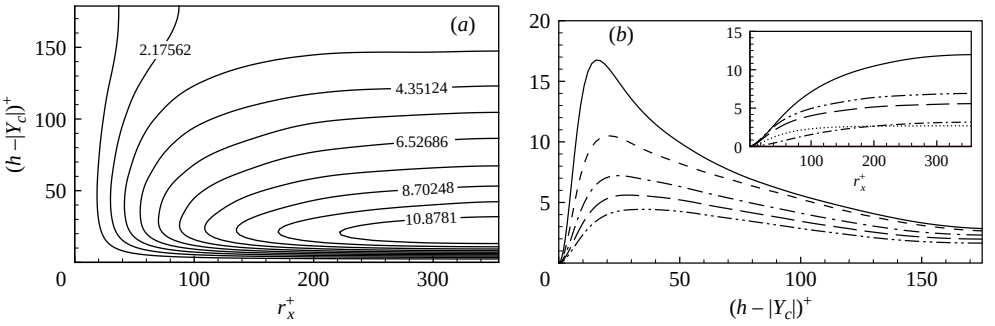

FIGURE 4. (*a*) Isolines of the scale energy $\langle \delta u^2(r_x, 0, 0|Y_c)\rangle$, normalized by u_*^2, in the (r_x^+, Y_c^+)-plane. (*b*) $\langle \delta u^2(r_x, 0, 0|Y_c)\rangle$ vs. $(h - |Y_c|)^+$ for different r_x: $r_x^+ = 55$ (dashed-double dotted line), $r_x^+ = 70$ (long dashed line), $r_x^+ = 100$ (dashed-dotted line), $r_x^+ = 220$ (dashed line). The solid line is $2(u_{rms}^2 + v_{rms}^2 + w_{rms}^2)$. Inset: $\langle \delta u^2(r_x, 0, 0|Y_c)\rangle$ vs. r_x^+ for different $(h - |Y_c|)$: $(h-|Y_c|)^+ = 4$ (dashed-dotted line), $(h-|Y_c|)^+ = 20$ (solid line), $(h-|Y_c|)^+ = 80$ (dashed-double dotted line), $(h - |Y_c|)^+ = 100$ (long dashed line), $(h - |Y_c|)^+ = 180$ (dotted line).

the main part of figure 4(*b*) for fixed separations. The plots corresponds to Y_c-sections of the (r_x, Y_c)-plane shown in (*a*). Overall the scale energy presents a maximum in the buffer layer which is sharper for larger separations but becomes smoother as r_x is reduced. The traditional plots showing the r_x-behaviour for fixed Y_c are shown in the inset. At large separations, where the velocities at the two points are uncorrelated, the limiting behaviour is given by $2\,(u_{rms}^2 + v_{rms}^2 + w_{rms}^2)$, i.e. four times the total turbulent kinetic energy pertaining to the considered value of Y_c. This quantity is represented by the solid line as a function of Y_c in the main panel of figure 4(*b*).

3.1. *Homogeneous flows*

In the simplest case of stationary homogeneous isotropic turbulence only the energy cascade and dissipation are relevant and the scale-energy balance at different scales is described by the classical Kolmogorov equation

$$\frac{\partial \langle \delta u^2 \delta u_i \rangle}{\partial r_i} = -4\langle \epsilon \rangle + 2\nu \frac{\partial \langle \delta u^2 \rangle}{\partial r_i \partial r_i}. \tag{3.1}$$

As is well known, in the inertial range the viscous correction is negligible and the turbulent component of the energy flux through scales $\langle \delta u^2 \delta u_\parallel \rangle = \langle \delta u^2 \delta u_i \rangle r_i / r$ is balanced by the energy dissipation (Frisch 1995). At smaller and smaller scales, the inertial contribution becomes less and less important, so that the dissipation is balanced by the viscous diffusion term. This picture is claimed to be highly universal, in the sense that, no matter what the details of the flow are at large scales, the small scales of large-Reynolds-number flows are believed to behave according to the balance established by the Kolmogorov equation (3.1). In its universality, equation (3.1) deliberately neglects the details of the process which feeds the turbulence to provide the constant energy flux though the inertial range.

The next step, in a sequence of increasingly complex flows, is represented by the homogeneous shear flow. In this case, besides energy transfer, viscous diffusion and dissipation, the additional process of energy production is explicitly taken into account. This prototypical flow, with several aspects idealized as much as homogeneous isotropic turbulence, isolates the turbulence production mechanism due to the mean

shear. The appropriate form of the Kolmogorov equation is

$$\frac{\partial\langle\delta u^2\delta u_i\rangle}{\partial r_i}+\frac{\partial(\langle\delta u^2\rangle Sr_y)}{\partial r_x}+2S\langle\delta u\delta v\rangle=-4\langle\epsilon\rangle+2\nu\frac{\partial\langle\delta u^2\rangle}{\partial r_i\partial r_i},\tag{3.2}$$

where y is the direction of the shear $S=\mathrm{d}U/\mathrm{d}y$, with a mean velocity $U(y)=Sy$ in the x-direction, and u and v are the components of the fluctuation velocity in direction x and y, respectively. The inertial transfer term for the fluctuations is split into two contributions: one due to the fluctuating field; the other associated with the mean flow – in this case the increment of the mean velocity field is $\delta U_i=Sr_y\delta_{i1}$. The process of energy production, represented by the term $2S\langle\delta u\delta v\rangle$, alters the classical balance and introduces a new scale ℓ_c defined as the cross-over between the convective energy flux and the production term (Casciola *et al.* 2003). The cross-over scale, dimensionally related to the so-called shear scale $L_s=\sqrt{\langle\epsilon\rangle/S^3}$, splits the inertia-dominated range into a classical inertial range at small scales, where equation (3.1) is recovered, from a production-dominated range at large scales. Below ℓ_c one may model the dynamics by means of equation (3.1) completed with an assigned incoming energy flux at scales $O(\ell_c)$.

3.2. *Scale-energy budget for a simple shear*

Inhomogeneity poses a new challenge in understanding turbulent dynamics, by introducing spatial transfer terms and by spatially modulating the balance. The extension of the Kolmogorov equation to inhomogeneous conditions can be achieved following the procedure described by Hill (2002), see also Yakhot (2001) and Kurien & Sreenivasan (2001) for an alternative approach. The two geometrical points where the relevant velocity increment $\delta u_i=u_i'-u_i$ is evaluated are expressed as $x_i'=X_{ci}+r_i/2$ and $x_i=X_{ci}-r_i/2$. After lengthy calculations the final equation is (for a detailed derivation see Hill 2002)

$$\begin{aligned}\frac{\partial\langle\delta u^2\delta u_j\rangle}{\partial r_j}+\frac{\partial\langle\delta u^2\delta U_j\rangle}{\partial r_j}+2\langle\delta u_i\delta u_j\rangle\frac{\partial\delta U_i}{\partial r_j}+\frac{\partial\langle u_j^*\delta u^2\rangle}{\partial X_{cj}}+\frac{\partial\langle\delta u^2U_j^*\rangle}{\partial X_{cj}}\\+2\langle u_j^*\delta u_i\rangle\frac{\partial\delta U_i}{\partial X_{cj}}=-4\langle\epsilon^*\rangle+2\nu\frac{\partial^2\langle\delta u^2\rangle}{\partial r_j\partial r_j}-\frac{2}{\rho}\frac{\partial\langle\delta p\delta u_i\rangle}{\partial X_{ci}}+\frac{\nu}{2}\frac{\partial^2\langle\delta u^2\rangle}{\partial {X_{cj}}^2},\end{aligned}\tag{3.3}$$

where an asterisk denotes a mid-point average, e.g. $u_i^*=(u_i(x_s')+u_i(x_s))/2$, and as before, δ denotes an increment, e.g. $\delta U_i=U_i(x_s')-U_i(x_s)$.

For a simple shear with mean velocity $U(y)$ in the x-direction equation (3.3) specializes to

$$\begin{aligned}\frac{\partial\langle\delta u^2\delta u_i\rangle}{\partial r_i}+\frac{\partial\langle\delta u^2\delta U\rangle}{\partial r_x}+2\langle\delta u\delta v\rangle\left(\frac{\mathrm{d}U}{\mathrm{d}y}\right)^*+\frac{\partial\langle v^*\delta u^2\rangle}{\partial Y_c}\\=-4\langle\epsilon^*\rangle+2\nu\frac{\partial^2\langle\delta u^2\rangle}{\partial r_i\partial r_i}-\frac{2}{\rho}\frac{\partial\langle\delta p\delta v\rangle}{\partial Y_c}+\frac{\nu}{2}\frac{\partial^2\langle\delta u^2\rangle}{\partial {Y_c}^2},\end{aligned}\tag{3.4}$$

which is the starting point for the present analysis of inhomogeneity effects on turbulent fluctuations in a channel flow.

Equations (3.3) and (3.4) were originally conceived in terms of the two spatial variables (x_i', x_i). The change of variables to the new set (X_{ci}, r_i) allows us to directly recover Kolmogorov equation (3.1) as homogeneous isotropic conditions are approached. In this remapping, the X_{ci} dependence is naturally associated with inhomogeneity, since, for homogeneous flows each term containing derivatives with respect to the mid-point vanishes and equation (3.4) reduces to (3.2).

3.3. *The behaviour at large scales*

Equations (3.3) and (3.4) manifest a well-defined asymptotic behaviour as larger and larger scales are approached. For $r \gg \ell$, where ℓ is the relevant correlation length, quantities evaluated at x_i and x_i' are uncorrelated and equation (3.3) reduces, within a factor 4, to the mid-point average of the single-point energy budget (2.1). In this respect, equation (2.1) is contained in the more general scale-energy budget (3.4) as a limiting case.

More specifically, at large scales we observe that

$$\lim_{r\to\infty} \frac{\partial \langle \delta u^2 \delta u_k \rangle}{\partial r_k} = \frac{1}{2}\left(\frac{\partial \langle u^2 u_k \rangle}{\partial x_k} + \frac{\partial \langle u'^2 u_k' \rangle}{\partial x_k'} \right) = \frac{\partial \langle u^2 u_k \rangle^*}{\partial X_{c_k}}, \tag{3.5}$$

where $\partial/\partial r_k = \frac{1}{2}(\partial/\partial x_k' - \partial/\partial x_k)$ and $\partial/\partial X_{c_k} = (\partial/\partial x_k' + \partial/\partial x_k)$. For homogeneous flows, the right-hand side of equation (3.5) is zero, and the divergence in r-space of the turbulent component $\langle \delta u^2 \delta u_k \rangle$ of the scale-energy flux vanishes as the separation is increased. At this condition the turbulent flux also vanishes since

$$\lim_{r\to\infty} \langle \delta u^2 \, \delta u_k \rangle = \delta \, \langle u^2 \, u_k \rangle. \tag{3.6}$$

This implies, e.g., that in the homogeneous shear flow the energy cascade is initialized at finite separations by the displacement towards small scales of the energy provided by the production term. Similarly, the Kolmogorov equation stated in the form (3.1) necessarily requires a feeding of the energy flux at finite separations. This boundary condition on the energy flux is frequently enforced by introducing a stochastic forcing acting at large but finite scales.

In this context, large-scale inhomogeneity introduces an additional feature which is particularly significant for wall-bounded flows, where strong y dependence is expected. For instance, for a channel flow, given a separation vector in the wall-parallel plane $(r_x, 0, r_z)$, equation (3.5), as r increases, yields $\partial \langle \delta u^2 \delta v \rangle / \partial r_y \to \mathrm{d}\langle u^2 v \rangle / \mathrm{d}y$, which corresponds to twice the turbulent transport term of the turbulent kinetic energy budget (2.1). As shown in figure 3(*a*) this turbulent convection term, which is significant in the entire channel section, enforces the large-scale boundary condition for the r-space divergence of the scale-energy flux. Concerning the asymptotic behaviour of equation (3.4), one cannot miss that a factor 2 is still needed in order to recover the correct result given by four times the transport term in the turbulent kinetic energy equation. This contribution, which stems from $\partial/\partial Y_c \langle v^* \delta u^2 \rangle$, is discussed in § 4.

4. Fluxes of scale energy

Formally the scale-energy budget (3.4) can be recast as

$$\nabla_r \cdot \boldsymbol{\Phi}_r(\boldsymbol{r}, Y_c) + \frac{\mathrm{d}\Phi_c(\boldsymbol{r}, Y_c)}{\mathrm{d}Y_c} = s(\boldsymbol{r}, Y_c), \tag{4.1}$$

where $\boldsymbol{r} = (r_x, r_y, r_z)$ and boldface type denotes a three-dimensional vector.

In the conservation form (4.1) two kinds of scale-energy fluxes exist, namely $\boldsymbol{\Phi}_r$ in the space of scales and Φ_c in geometrical space. The source term,

$$s(\boldsymbol{r}, Y_c) \; = \; -2\langle \delta u \delta v \rangle (\mathrm{d}U/\mathrm{d}y)^* - 4\langle \epsilon^* \rangle, \tag{4.2}$$

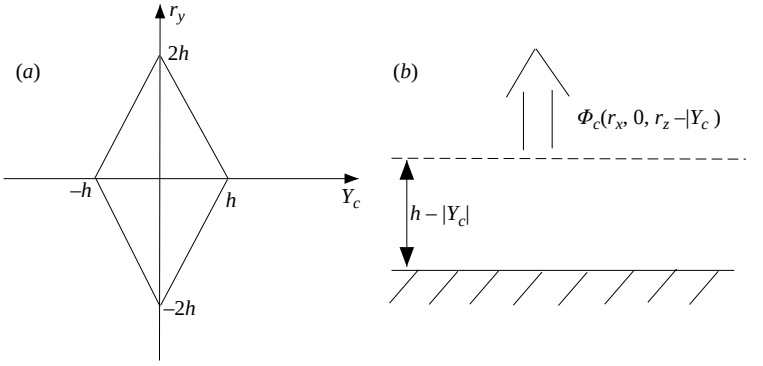

FIGURE 5. (*a*) Integration domain for equation (4.1). (*b*) Physical interpretation of the spatial flux $\Phi_c(r_x, 0, r_z|Y_c)$.

accounts for production due to shear and dissipation. Various contributions to the fluxes can be identified,

$$\Phi_c(\boldsymbol{r}, Y_c) = \langle \delta u^2 v^* \rangle + \frac{2}{\rho}\langle \delta p \delta v \rangle - \frac{\nu}{2}\frac{\mathrm{d}\langle \delta u^2 \rangle}{\mathrm{d}Y_c}, \tag{4.3}$$

$$\boldsymbol{\Phi}_r(\boldsymbol{r}, Y_c) = \langle \delta u^2 \delta \boldsymbol{u} \rangle + \langle \delta u^2 \delta \boldsymbol{U} \rangle - 2\nu \nabla_r \langle \delta u^2 \rangle, \tag{4.4}$$

in principle related to turbulent transport, transport by the mean flow (absent in Φ_c), viscous diffusion and, only in Φ_c, pressure–velocity correlation.

The integration domain for equation (4.1), corresponding to the constraint $-h \leqslant y,\ y' \leqslant h$, i.e. to the geometry of the channel flow, is

$$-h \leqslant Y_c \leqslant h, \qquad -2(h - |Y_c|) \leqslant r_y \leqslant 2(h - |Y_c|), \tag{4.5}$$

see figure 5(*a*).

The spatial flux describes the transport of scale energy in geometric space and is, in principle, a three-dimensional vector – see equation (3.3) – that could be denoted by the boldface type $\boldsymbol{\Phi}_c$. For a channel flow the only non-vanishing component of $\boldsymbol{\Phi}_c$, namely the scalar Φ_c appearing in (4.1), corresponds to a transfer of energy at scale r in the y-direction, i.e. towards the wall or towards the bulk of the flow according to its sign. In fact, after setting $r_y = 0$ and accounting for the boundary conditions, term-by-term integration of equation (4.1) from the (lower) wall to the current value of Y_c,

$$\Phi_c(r_x, 0, r_z|Y_c) = \int_{-h}^{Y_c} [\, s(r_x, 0, r_z|\tilde{Y}_c) - \nabla_r \cdot \boldsymbol{\Phi}_r(r_x, 0, r_z|\tilde{Y}_c)\,]\, \mathrm{d}\tilde{Y}_c, \tag{4.6}$$

leads to the interpretation of $\Phi_c(r_x, 0, r_z|Y_c)$ as the amount of scale energy which leaves the region below Y_c to feed the portion of the channel above, see figure 5(*b*) for a sketch.

4.1. *The r-averaged equation*

When discussing the Kolmogorov equation for homogeneous flows, (3.1), it is customary to consider its r-averaged form obtained by integrating the equation over a ball of radius r in the space of scales. The procedure highlights the role of the energy flow across scales, $\boldsymbol{\Phi}_r$, and leads to the classical form of the Kolmogorov equation in terms of longitudinal velocity increments.

An analogous procedure can be used in principle for the generalized form (4.1) for unbounded flows which, in r-averaged form, would be

$$\frac{1}{V_r}\int_{\partial B_r} \boldsymbol{\Phi}_r(\boldsymbol{r},\, Y_c)\cdot \boldsymbol{n}_r \,\mathrm{d}S_r + \frac{1}{V_r}\int_{B_r} \frac{\mathrm{d}\Phi_c(\boldsymbol{r},\, Y_c)}{\mathrm{d}Y_c}\,\mathrm{d}V_r \,=\, \frac{1}{V_r}\int_{B_r} s(\boldsymbol{r},\, Y_c)\,\mathrm{d}V_r, \quad (4.7)$$

where $\boldsymbol{n}_r$ is the outward normal to the ball B_r with radius r and volume V_r. This integral form identifies $\boldsymbol{\Phi}_r$ as a transfer of scale energy among scales above and below r. A negative value of $\boldsymbol{\Phi}_r \cdot \boldsymbol{n}_r$ implies that scale energy is transferred inside the ball from the exterior, i.e. we are in the presence of the classical direct, or forward, cascade of Richardson. In homogeneous isotropic turbulence, at inertial separation one recovers

$$\frac{1}{V_r}\int_{\partial B_r} \boldsymbol{\Phi}_r(\boldsymbol{r})\cdot \boldsymbol{n}_r \,\mathrm{d}S_r \,\propto\, \frac{\langle\, \delta u_\parallel^3 \,\rangle}{r} < 0, \quad (4.8)$$

which gives the well known four-fifths law.

When dealing with the geometry of the channel, however, the integration over a sphere is unsuitable for two main reasons. First, spheres with radius r exceeding the distance from the wall $2\,\big(h-|Y_c|\big)$ are not entirely contained within the flow region, see the integration domain (4.5) sketched in figure 5. Secondly, averaging over a sphere implies averaging in the wall-normal direction which is undesirable for a flow with a strong y-dependence. To overcome these drawbacks, we consider r-averaging on two-dimensional square domains of side r belonging to wall parallel planes, according to the expression

$$Q_r(r, Y_c) = \frac{1}{r^2}\int_{-r/2}^{r/2}\int_{-r/2}^{r/2} q(r_x, 0, r_z|Y_c)\,\mathrm{d}r_x\mathrm{d}r_z, \quad (4.9)$$

where q denotes a generic quantity.

When applying the r-averaging operator (4.9), the contribution from the second term on the left-hand side of equation (3.4) vanishes altogether, since $\delta U = 0$ when $r_y = 0$. The r-averaged form of the equation then follows as

$$T_r(r, Y_c) + \Pi(r, Y_c) + T_c(r, Y_c) = E(r, Y_c) + D_r(r, Y_c) + P(r, Y_c) + D_c(r, Y_c) \quad (4.10)$$

where each term corresponds to the appropriate term in (3.4). Specifically, T_r gives the inertial contribution to the scale-energy flux in r-space, which is proportional to $\langle \delta u_\parallel^3 \rangle / r$ for homogeneous isotropic turbulence. Π arises from the first contribution to the source term s, which is due to production. This term is already present in the homogeneous shear flow. T_c is the inertial contribution to the spatial flux of scale energy and it is strictly associated with inhomogeneity. E is the term related to dissipation which arises from the second contribution to the source s. D_r and D_c are the diffusive components of the flux in r-space and in geometric space, respectively, and, finally, P is an inhomogeneous contribution related to the pressure–velocity correlation.

4.2. *Spatial redistribution of energy*

We analyse first the spatial component of the scale-energy flux Φ_c. Figure 6(a) plots the r-space average of $\Phi_c(\boldsymbol{r}, Y_c)$, according to definition (4.9), as a function of the distance from the wall for different values of the separation r. Two well-separated regions where the spatial scale-energy flux is negative and positive, respectively, are apparent. Where it is negative, the spatial flux transfers scale energy towards the wall; where it is positive, towards the bulk of the flow. The sustainment of turbulence for

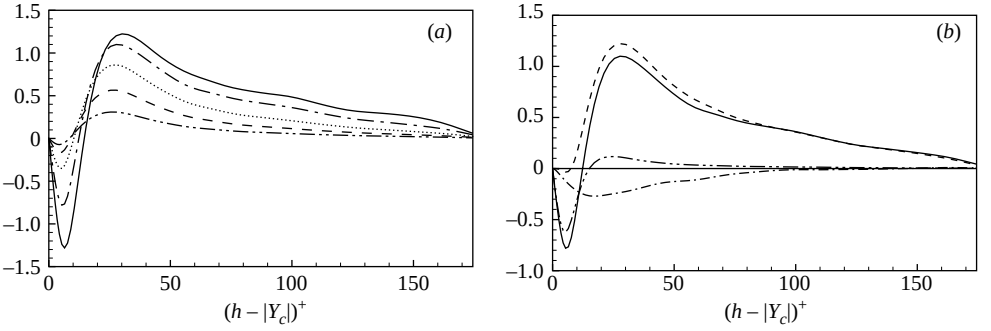

FIGURE 6. (*a*) The r-space average of Φ_c as a function of the distance from the wall $(h-|Y_c|)^+$ for different values of the scale r^+: $r^+ = 5$ (— · · —), $r^+ = 10$ (——), $r^+ = 20$ (· · ·), $r^+ = 40$ (— · —), $r^+ = 120$ (——). The r-space average is performed on two-dimentional square domains (r_x, r_z), with side r at $Y_c = \text{const}$ and $r_y = 0$. (*b*) Different contributions to the r-space average of Φ_c, see equation (4.3), as a function of $(h-|Y_c|)^+$ for fixed separation $r_+ = 40$. Φ_c(——), viscous diffusion (— · · —), pressure transport (— · —), turbulent flux (——).

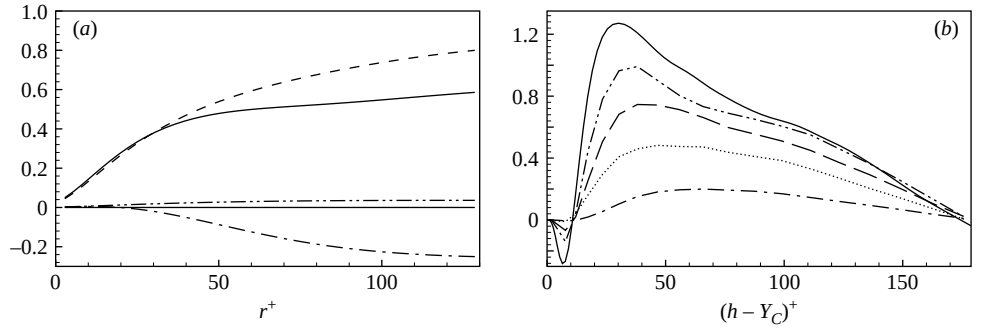

FIGURE 7. (*a*) Different contributions to the r-space average of Φ_c, see equation (4.3), vs. separation r^+ for $(h-|Y_c|)^+ = 80$. Φ_c(——), viscous diffusion (— · · —), pressure transport (— · —), turbulent flux (——). (*b*) Turbulent transport of scale energy (non-averaged) $\langle \delta u^2 v^* \rangle$ vs. distance from the wall $(h-|Y_c|)^+$ for different separations, $r_+ = 20$ (— · —), $r_+ = 40$ (· · ·), $r_+ = 80$ (——), $r_+ = 170$ (— · · —). The solid line corresponds to twice the turbulent energy flux $(\frac{1}{2}\langle u^2 v \rangle)$, see (2.1), according to the limiting behaviour (4.11).

all scales is partially due to a spatial transport of scale energy generated in the buffer layer. However the importance of this process will change depending on both the specific scale and the geometric location considered. This issue will be treated in full detail in the next section.

Figure 6(*b*) displays the different contributions to the r-average of Φ_c at $r^+ = 40$. The spatial flux (solid line) changes sign at $(h-|Y_c|)^+ \simeq 15$, which closely corresponds to the location of the maximum turbulent kinetic energy production. For $(h-|Y_c|)^+ > 15$ the most important contribution is provided by the turbulent transport, the first term in definition (4.3) (dashed lines in figure 6*b*). This is confirmed by inspection of figure 7(*a*) which plots the same quantities, now as functions of the separation r at $(h-|Y_c|)^+ = 80$. In the large-scale limit, all terms tend to an asymptotic value determined by the corresponding terms in the turbulent kinetic energy equation (2.1), as discussed in § 3.3. Below $(h-|Y_c|)^+ = 15$ the most significant contribution to Φ_c is given by the viscous diffusion, the last term in the definition (dash-double dotted

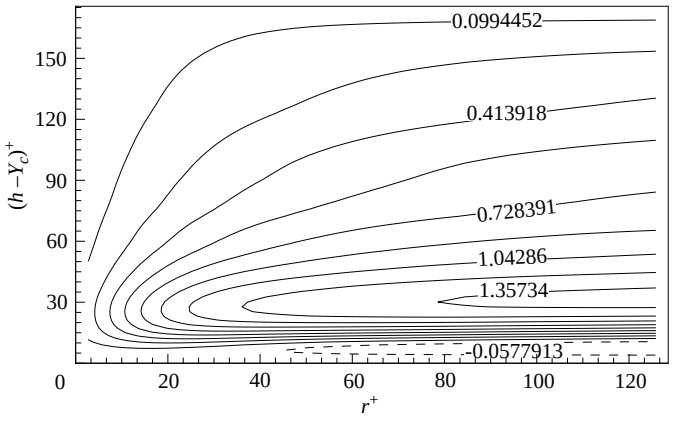

FIGURE 8. The r-space average of the turbulent transport of scale energy $\langle \delta u^2 v^* \rangle$, normalized by u_*^3, as a function of the distance from the wall $(h-|Y_c|)^+$ and of the scale r^+. The uniformly spaced contour levels are shown by solid and dashed lines for positive and negative values, respectively.

line in figure 6*b*). Across the buffer layer, up to the lower part of the log-region, the pressure-velocity correlation also contributes significantly (the second term in (4.3)).

Let us consider in more detail the turbulent component of the spatial flux $\langle \delta u^2 v^* \rangle$ addressed – in its non-averaged form – in figure 7(*b*) which displays $\langle \delta u^2 v^* \rangle (r_x, 0, 0|Y_c)$ as a function of $(h-|Y_c|)$ for increasing separations. In the limit of large separations one finds

$$\lim_{r \to \infty} \langle \delta u^2 v^* \rangle = \langle u^2 v \rangle^*, \tag{4.11}$$

which corresponds to twice the turbulent flux of the single-point kinetic energy budget (2.1) (solid line in figure 7). This provides the missing factor 2 in the large-r asymptotics discussed in § 3.3. A trend to form a plateau in correspondence with the log-layer can be guessed from the plots. In fact, as the Reynolds number is increased, $\langle u^2 v \rangle$ is known to approach a constant value in the log-layer, Moser *et al.* (1999). The same behaviour is expected concerning the turbulent component of Φ_c, namely $\langle \delta u^2 v^* \rangle$, implying that, for large Reynolds numbers, the log-layer is asymptotically traversed by an almost constant flux of scale energy.

Figure 8 shows the isolines of the r-space average of $\langle \delta u^2 v^* \rangle$. This is a function of two variables, namely the scale r and the position Y_c, and is represented by its contours for the reasons already mentioned for figure 4. The turbulent component of the spatial flux is clearly built-up in the buffer layer and is particularly significant at inertial separations. It reaches its maximum in the log-layer, to progressively decrease as the centreline of the flow is approached. This decrease implies that the amount of scale energy carried by the flux is progressively released to the fluctuations in the core region. Moreover, $\langle \delta u^2 v^* \rangle$ also contributes to feeding the viscous sublayer, as shown by its negative values near the wall. From the pattern of the isolines it is clear that vanishingly small values of the turbulent flux are attained close to the centreline of the channel. The same isolines pass close to the $(h-|Y_c|)$-axis, implying that at viscous separations – small r – the turbulent component of the spatial flux is negligible, as expected. The similarity between the gross features of figure 8, concerned with the r-averaged turbulent flux, and those of figure 4, giving the scale energy, is in a way understandable, since the two quantities are strictly related. In fact, both

plots highlight the crucial role of the large scales of the buffer layer, as the preferred location for the scale energy, for the scale-energy production and, consistently, for the turbulent component of the spatial flux discussed here.

5. Scale-by-scale budget

Let us now consider the detailed balance expressed by the r-averaged scale-energy budget (4.10). The effective amount of scale energy per unit time which is available at location Y_c is provided by the local production Π plus the r-averaged divergence of the spatial flux, Φ_c, minus the local dissipation E. This net rate of scale energy intake feeds the cascade across scales described by T_r. To ease the interpretation of the diagrams, it is instrumental to group together some terms of equation (4.10): we have decided to add together the contributions of inertial origin in a sort of effective production

$$\Pi_e(r,\, Y_c) \,=\, \Pi(r,\, Y_c) \,+\, T_c(r,\, Y_c) \,-\, P(r,\, Y_c). \tag{5.1}$$

It corresponds to the amount of scale energy made available at the particular scale and location by production and overall turbulent transport. Clearly, the single contributions are not positive definite, while their sum must be positive where turbulent energy stems from inertial mechanisms. Analogously, the contributions of diffusive nature have been added to form a modified dissipation rate,

$$E_e(r,\, Y_c) \,=\, E(r,\, Y_c) \,+\, D_r(r,\, Y_c) \,+\, D_c(r,\, Y_c), \tag{5.2}$$

as the sum of the actual dissipation and the diffusive fluxes of scale energy in physical and r-space, respectively. With these definitions, the r-averaged balance is expressed in more concise form as

$$T_r(r,\, Y_c) \,+\, \Pi_e(r,\, Y_c) \,=\, E_e(r,\, Y_c), \tag{5.3}$$

to be read as: transfer across scales plus effective production equals effective dissipation.

In the following, equation (5.3) and the different contributions to effective production and dissipation will be addressed on the basis of the traditional topology of the flow, see figure 2 and its caption. In describing the different regions, instead of the standard sequence, we prefer to follow this conceptual one: first we address the log-layer, which closely resembles the homogeneous shear flow. Secondly the bulk region, where substantial differences with respect to homogeneous-isotropic turbulence arise due to the spatial fluxes. Finally, after considering the viscous sublayer where the effect of viscosity is prevailing at all scales, we conclude by discussing the buffer layer which is considered as the engine of wall turbulence. The main results are shown in several figures with a common format, each pertaining to a different position. Let us describe their common structure, see e.g. figure 9. Panel (*b*) shows the components of the effective production Π_e defined in (5.1). The components of the effective dissipation, (5.2), are reported in the inset. All these quantities are plotted with a minus sign, to ease the comparison with panel (*a*) concerning the global budget, (5.3). The sum of T_r and Π_e is plotted there as symbols, while the solid line represent E_e. The imbalance between the right- and left-hand sides of (5.3), graphically given by the misplacement of the symbols with respect to the dashed line, is a measure of the statistical error in the data (see the Appendix). The cross-over point between T_r and Π_e is a central issue in the discussion of the results (see figure 3*b*). To better visualize its position the

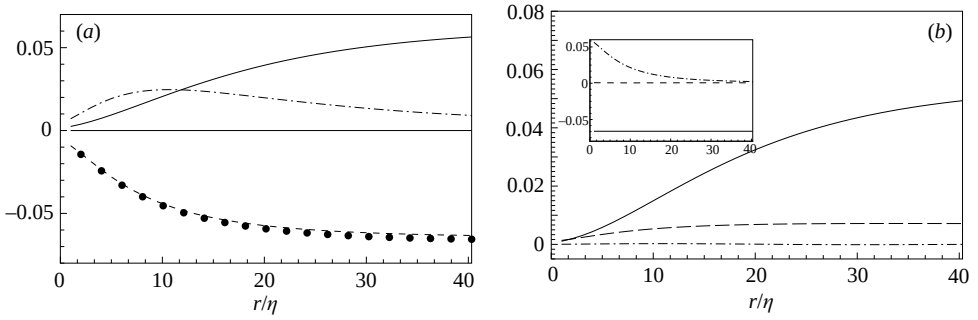

FIGURE 9. Detailed balance (5.3) in the log-layer, $(h-|Y_c|)^+=80$. (*a*) The sum $(T_r+\Pi_e)$ is represented by the filled circles, E_e is given by the dashed line. The solid line is $-\Pi_e$, the dash-dotted line corresponds to $-T_r$. (*b*) The different contributions to the effective production, $-\Pi_e$, (5.1), plotted as functions of the scale r, namely production $-\Pi$ (solid line), turbulent transport $-T_c$ (dashed line) and pressure transport $-P$ (dash-dotted line); note that the sign of each term has been changed. In the inset, the various terms of the effective dissipation E_e, (5.2): dissipation E (solid line) and diffusion of scale energy in physical and in r-space, D_c (dashed line) and D_r (dash-dotted line), respectively.

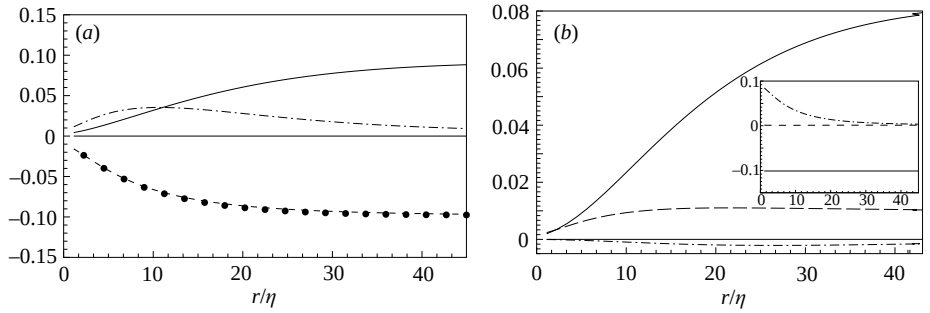

FIGURE 10. As figure 9 but at $(h-|Y_c|)^+=60$ (log-layer).

sign of these two terms has been changed to separate the relevant graph from other curves in the same panel.

5.1. *The log-layer*

We are now ready to analyse the log-layer. Figure 9 addresses the balance (5.3) for a typical location in this region, specifically $(h-|Y_c|)^+=80$. As anticipated, figure 9(*a*) shows the budget, which will be discussed in a while. Let us first analyse the different contributions to the effective production (5.1) displayed in figure 9(*b*). In the log-layer $\Pi_e\simeq\Pi$, since turbulent and pressure transport, T_c and P, respectively, are much smaller than Π, see also figures 10 and 11 corresponding to $(h-|Y_c|)^+=60$ and 100, respectively. The plots of the different terms contributing to the effective dissipation (5.2) are shown in the inset. As expected, in the log-layer the diffusive flux of scale energy in physical space, D_c, is very small while the corresponding term in r-space, D_r, is crucial at small scales, becoming negligible at inertial separations where $E_c\simeq E$. Overall, the dynamics is identical to that observed in the homogeneous shear flow discussed in Casciola *et al.* (2003), where the sum of the inertial component of the flux across scales, T_r (i.e. the energy cascade term), and production Π balances dissipation plus diffusion across scales. The detailed budget (5.3) is represented in figure 9(*a*), which plots the sum $(T_r+\Pi_e)$ in comparison with E_e. In the same figure

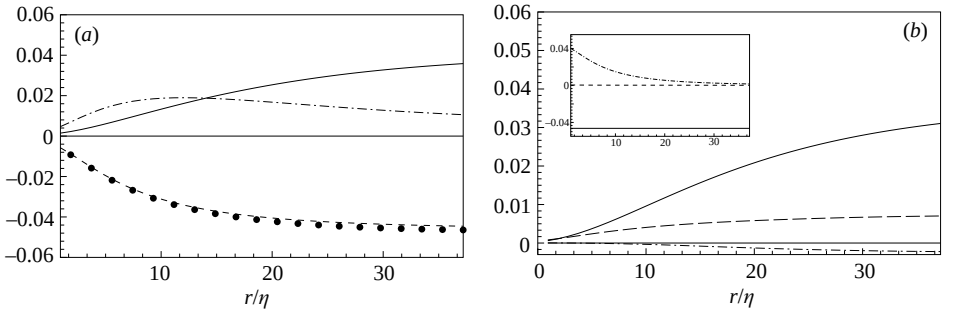

FIGURE 11. As figure 9 but at $(h-|Y_c|)^+ = 100$ (upper log-layer).

cascade and production terms are compared to establish the range of scales where each is most significant for the dynamics of turbulent fluctuations. Apparently, at large separations the production overwhelms the cascade term, and $\Pi > T_r$ down to a cross-over scale $\ell_c(Y_c)$ defined by the condition

$$\Pi(\ell_c, Y_c) = T_r(\ell_c, Y_c). \tag{5.4}$$

According to the classical equilibrium theory for the log-layer, the local dissipation can be estimated in terms of production of turbulent kinetic energy, $\langle\epsilon(y)\rangle \simeq u_*^3/(ky)$. By comparing the order of magnitude of the fluctuations induced at scale r by the shear, $\delta u_s(r) \simeq Sr$, with that typical of the classical Kolmogorov-like inertial range, $\delta u_K(r) \simeq \langle\epsilon\rangle^{1/3} r^{1/3}$, one is led to expect the cross-over between production-dominated and cascade-dominated range to occur at the shear scale $L_s = \sqrt{\langle\epsilon\rangle/S^3}$. Given the estimate for the dissipation, since $S(y) \simeq u_*/(ky)$, one finds the classical prediction $\ell_c(Y_c) \simeq k(h-|Y_c|)$. The cross-over scale (5.4) as function of the distance from the wall is reported in figure 3, which shows a remarkable agreement with the dimensional prediction.

Generally speaking, the dynamics of the log-layer, as the equilibrium region where global production and dissipation balance, reproduces the condition of a locally homogeneous shear. Above the cross-over scale, i.e. in the production range, the shear is able to energize the fluctuations; below ℓ_c the shear plays no significant role and the corresponding dynamics reduces to the classical Richardson cascade which is eventually terminated at the local dissipative scale by diffusion. Inhomogeneity plays here only a minor role expected to vanish with increasing Reynolds number. However, a substantial difference with the homogeneous shear flow is worth emphasizing: the log-layer is traversed by an almost constant flux of scale energy directed towards the bulk region of the flow. The viscous component is entirely negligible at all scales, with respect to the turbulent flux, see, e.g., figure 7(*a*). Despite the leading role of the turbulent flux in the log-layer, its divergence is sufficiently small in comparison with the other terms of the budget to be dynamically ineffective – see figures 9(*b*), 10(*b*), 11(*b*). The shape of the turbulent flux $\langle\delta u^2 v^*\rangle$ as a function of Y_c for fixed r is bounded by its limiting behaviour for $r \to \infty$, i.e. its shape at all scales is controlled by the turbulent transport term of the single-point turbulent kinetic energy equation – see the discussion concerning figure 7(*b*) in §4.2. As discussed e.g. by Moser *et al.* (1999), for increasing values of the Reynolds number, the turbulent kinetic energy flux should more and more approximate to a constant in the log-layer, inducing an identical behaviour in the turbulent transport of scale energy in Y_c-space. Hence its

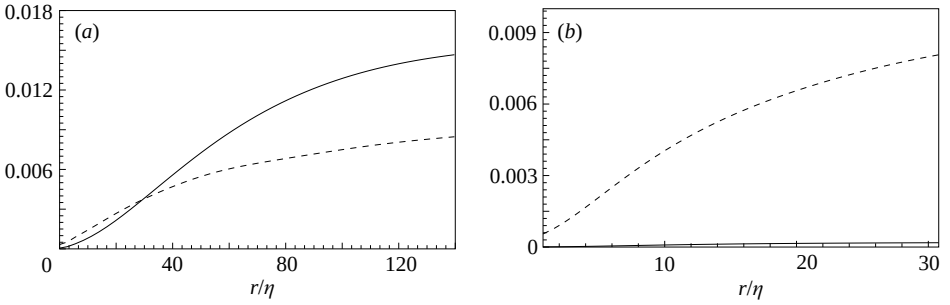

FIGURE 12. Production Π (solid line) and turbulent flux T_c (dashed line) of scale energy in the bulk region of the turbulent channel flow. (*a*) $(h-|Y_c|)^+ = 130$. (*b*) Centreline, $(h-|Y_c|)^+ = 180$.

divergence should become zero in the limit and the fact that in the present simulation it is not strictly zero should be regarded as a finite-Reynolds-number effect.

According to the above picture, the log-region appears as an equilibrium layer of essentially inviscid nature across which the scale energy is found to flow with no effective interference with the local dynamics. In particular, for scales dominated by the classical inertial terms, i.e. for $\eta \ll r \ll \ell_c$, see figure 3(*b*) to appreciate the extension of this range as a function of wall distance, two kinds of inviscid/turbulent fluxes of scale energy take place: one in physical space directed from the wall towards the bulk of the channel, the other in the space of scales, directed from the large towards the small scales.

5.2. *The bulk region*

In the log-layer, the production of scale energy Π is always much larger than the injection via turbulent and pressure transport, T_c and P in equation (5.1), respectively (see figures 9(*b*), 10(*b*) and 11(*b*)). As the bulk of the flow is approached the shear becomes smaller and smaller, entailing the drastic reduction of the local production term. The turbulent fluctuations are here mainly sustained by the divergence of the spatial turbulent flux of scale energy. Figure 12 provides a direct comparison between Π and T_c for the entire range of available scales at a location close to (panel(*a*), $(h - |Y_c|)^+ = 130$) and right at the channel centre (panel(*b*), $(h - |Y_c|)^+ = 180$). The corresponding plots should be analysed by recalling the results shown in figure 11(*b*), which displays the same quantities for the external part of the log-layer. In the log-layer the divergence of the turbulent flux of scale energy is always sub-leading with respect to the local production. As the bulk of the flow is approached, the production of scale energy still remains predominant at large scales, while a significant amount of scale energy at small scales begins to be supplied by the wall-normal turbulent flux, see figure 12(*a*). On reaching the centreline the production should exactly vanish uniformly through the entire range of scales, so that the entire amount of scale energy carried by the spatial flux now feeds the turbulence, see figure 12(*b*) giving the relevant components of the effective production on the symmetry line.

The detailed balance at the centreline, $(h - |Y_c|)^+ = 180$, is shown in figure 13(*a*). The effective production, essentially given by the divergence of the turbulent flux T_c, is systematically less than the turbulent flux across scales, represented by T_r. Their sum equals the effective dissipation, whose components are plotted in the inset of figure 13(*b*). Intuitively, the bulk region is also an inertia-dominated region where viscosity only acts on the dissipative scales of the flow through the viscous component

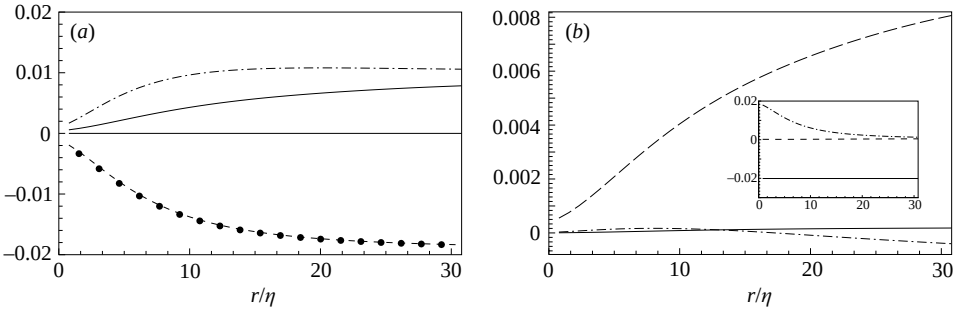

FIGURE 13. As figure 9 but in the bulk region, $(h-|Y_c|)^+ = 180$.

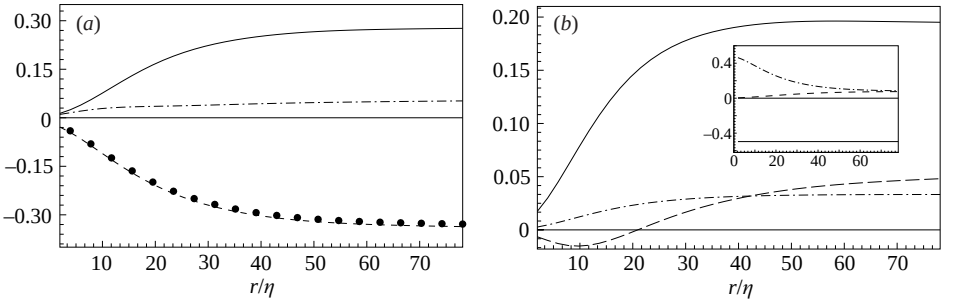

FIGURE 14. As figure 9 but in the sublayer, $(h-|Y_c|)^+ = 3$.

D_r of the scale-energy flux across scales. A specific feature of the channel centreline, $Y_c = h$, is that, at large separations, effective production equals turbulent flux across scales, namely

$$\lim_{r\to\infty} T_r(r,h) \;=\; \lim_{r\to\infty} \Pi_e(r,h), \tag{5.5}$$

where the common limit is given by half the effective dissipation $E_e(r,h)$, as shown for large r in figure 13(a). This is a straightforward consequence of the symmetry of the flow, which implies $\Pi = 0$, and the limiting behaviours (3.5) and (4.11).

5.3. *The viscous sublayer*

In § 4.2 the viscous sublayer has been shown to receive scale energy from above through the flux of energy, Φ_c, which is directed towards the wall. As shown in figure 6(b), the predominant contribution to the r-averaged value of Φ_c is provided by the viscous diffusion term. Its divergence, i.e. its Y_c-derivative D_c, contributes to the effective dissipation E_e as defined in equation (5.2). For $(h-|Y_c|)^+ = 3$ this term is shown in the inset of figure 14(b). In fact, D_c provides only a small contribution to the effective dissipation, significant mostly at large scales. Concerning small scales, as everywhere else in the channel, the behaviour of E_e is determined by the actual dissipation and by the scale diffusion D_r. Figure 14(b) displays, as usual, the different terms of the effective production Π_e. Most of the scale energy made available to the fluctuations in the sublayer is generated by the genuine production term Π which operates via the local shear. However, turbulent and pressure transport contribute to a significant extent. In fact, despite the fact that turbulent and pressure transport contributions to Φ_c are relatively small in the viscous sublayer their strong Y_c dependence generates a non-negligible divergence and contributes a significant part of Π_e.

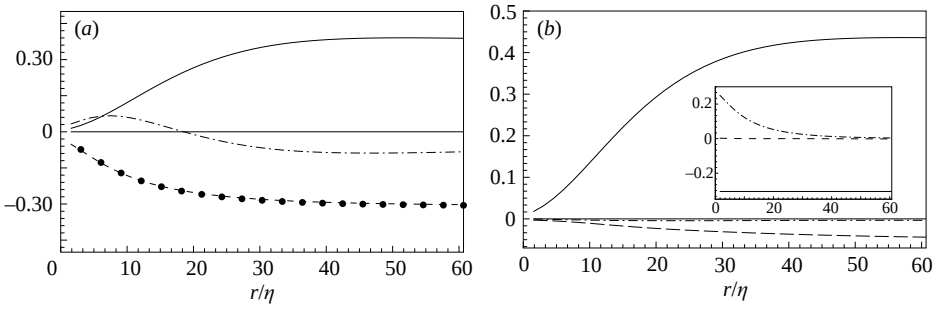

FIGURE 15. As figure 9 but in the buffer layer, $(h - |Y_c|)^+ = 20$.

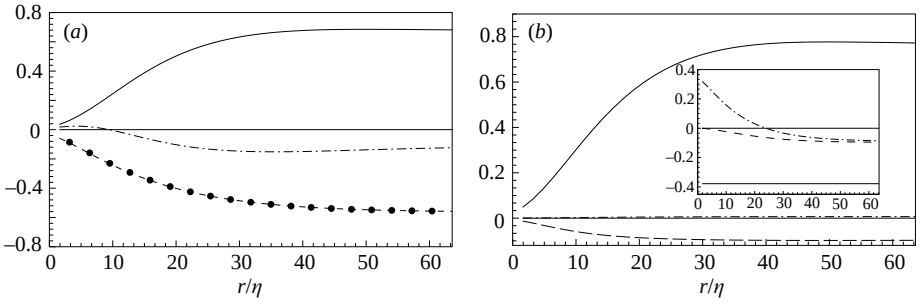

FIGURE 16. As figure 9 but at $(h - |Y_c|)^+ = 10$ (buffer layer).

The detailed balance is described by figure 14(a). In rough terms, the modified dissipation is counterbalanced by the modified production. The spatial transfer of scale energy, found to be crucial for the sustainment of the turbulence in the bulk region where no production occurs, is here less important since most of the energy is generated locally. Concerning the behaviour in the space of scales, a similar comment applies: the inertial transfer across scales plays a less significant role, with production and dissipation mostly taking place locally in the space of scales, in agreement with the well-established idea that, very close to the wall, viscosity is relevant at all scales.

5.4. *The buffer layer*

After the previous discussion of the log, the viscous and the bulk region, we are now ready to describe in detail the dynamics of the buffer layer, where most of turbulence activity is originated. According to the classical description, the buffer is identified with the transition region from the near-wall asymptotics of the viscosity-dominated sub-layer to the essentially inviscid scaling which characterizes the log-layer. This smooth transition is reproduced in the different terms of the scale-energy balance, as shown by the comparison of figure 15, deep within the buffer, with figure 16, close to the viscous sublayer, and with figure 17, in the low log-layer, respectively.

A more physically oriented discussion points out the role of the buffer layer as the effective engine of turbulent fluctuations in wall-bounded flows. This already emerges from the standard approach in terms of single-point statistics, which describes the buffer as the region where production exceeds dissipation, thereby implying that turbulent kinetic energy is irradiated towards the remaining parts of the flow. The more detailed scale-by-scale balance, see figure 15(a), confirms the above conclusion. In the effective production, the turbulent transport T_c reduces the amount of scale energy per unit time which is locally made available. Namely, it exactly corresponds

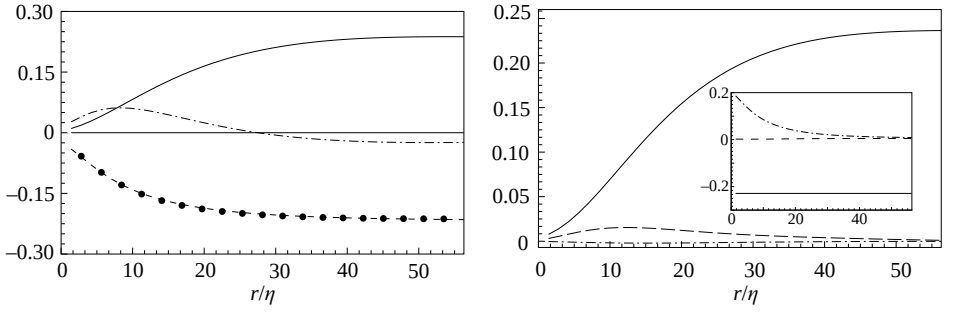

FIGURE 17. As figure 9 but at $(h - |Y_c|)^+ = 30$ (upper buffer layer).

to the scale energy which is drained from the specific location to contribute to the feeding of the adjacent regions. Concerning the effective dissipation E_e, the inset in figure 15(b) shows that the spatial diffusion term D_c is not particularly significant while in the detailed balance (figure 15a) the predominant term is the effective production, i.e. the local production Π amended from the spatial transport T_c.

A peculiar aspect of the buffer layer is the turbulent transport across scales T_r, which changes its nature from same sign as the local production at small scales to the opposite sign at large scales; in the figures, the sign of both T_r and Π_e has been changed for better readability of the plots. This behaviour should be interpreted in the sense of a classical cascade of energy occurring in the small scales which turns into a reverse cascade at large separations. Actually, the asymptotics of the turbulent flux across scales (3.5), by linking the large-scale behaviour of T_r to the transport term of turbulent kinetic energy, implies a positive limit (negative in figure 15 where T_r and Π_e are plotted with the opposite sign) as r increases, i.e. a reverse cascade. In this respect, the different features of the buffer layer – namely the ability to provide the excess of scale energy to the nearby regions by means of a spatial flux (i.e. its divergence T_c), the reverse cascade occurring in the space of scales at large separations (i.e. T_r) and the turbulent component of the flux of kinetic energy, see (2.1) – appear as strictly related aspects. Such processes may be conjectured as directly related to the dynamics of the coherent structures which are required to built up Reynolds stresses and present a definite cycle consisting of regeneration of relatively extended structures with quasi-periodic breakdown to small-scale turbulence.

In more detail, in the low-buffer region T_r is substantially positive at every scale, see $-T_r$ in figure 16, a behaviour presumably related to the low- and high-speed streaks which populate this area, Robinson (1991). Moving away from the wall towards the log-layer, the small scales begin to follow the classical cascade with energy flowing towards the dissipative range, while a tendency towards an inverse cascade is definitely maintained at large scales; this is presumably the imprint of the breakdown, regeneration and coalescence of the streamwise vortices, Hamilton *et al.* (1995). On entering the log-layer, no substantial focusing of turbulent kinetic energy occurs and the energy keeps cascading towards the dissipative range in the entire range of separations.

6. Concluding remarks

Two of the most important results in turbulence theory concern the idealization of the flow aimed, on the one hand, at the dynamics of the small scales and, on

the other, at the description of the near-wall layer of wall-bounded flows. The two theories are, in a sense, the complements of each other. The dual nature arises from the fact that, in the first case, the description is given in the space of scales – the separation r or, equivalently, the wavenumber – while in the other it is given in physical space. The question is how they can be reconciled in the non-ideal case of inhomogeneous/anisotropic flows at finite Reynolds number where an energy cascade and spatial momentum transfer occur simultaneously and asymptotic conditions are far from being reached. One should be able to address the dynamics of a given scale by evaluating the amount of energy income due to local production and spatial redistribution. We have used for this purpose an approach based on a generalized form of the Kolmogorov equation, originally derived by Hill (2002), to address the dynamics of wall-bounded turbulence as described by a low-Reynolds-number DNS of turbulent channel flow.

In physical terms, the generalized Kolmogorov equation directs the attention to the energy content of a given scale of turbulent motion as a function of the distance from the wall. Two different kinds of scale energy fluxes are identified, one related to the transport of scale energy in physical space, the other related to the transfer of energy across the spectrum of turbulent scales. The former is the natural extension of the classical flux of turbulent kinetic energy across the channel to a scale-by-scale context. The other takes care of the different forms of energy transfer which may occur in a complex turbulent flow, thus generalizing the concept of an energy cascade in homogeneous-isotropic turbulence. A certain scale at a given position in space receives turbulent energy by three different mechanisms: scale energy can be intercepted from the spatial flux, it can be drained from the inter-scale transfer and, finally, energy can also be generated locally by the interaction with the mean flow or by possible external agencies. In steady conditions, the balance implies that the net time rate of available scale energy should correspond to the local dissipation.

Each kind of scale-energy flux possesses two entirely different contributions: inertial and diffusive. Correspondingly, the range of the associated independent variable is split into subranges, dominated either by the diffusive or by the inertial component of the respective energy flux.

Our results show that the decomposition of the channel in terms of viscous layer, buffer region, log-layer and bulk region also maintains a well-defined meaning in the context of a scale-by-scale budget. The buffer layer appears as the region where production of scale energy is predominant and feeds the spatial flux towards adjacent zones. The log-layer corresponds to the equilibrium layer where production and dissipation balance, in the sense that, for each scale, energy is not received from nor released to the wall-normal spatial flux. The spatial flux of scale energy is instead crucial for turbulence sustainment in the bulk region. In fact, the excess production in the buffer layer crosses the log-layer as an essentially constant spatial flux to reach the bulk of the flow. In the space of scales, typically, the large-scale production range is followed by a nearly classical transfer range, closed by diffusion at the local dissipative scales. This description is particularly suited to the log-layer, for which the production range almost entirely feeds the local cascade process in the same way as for the homogeneous shear flow.

The existence of a coupled transfer of energy occurring simultaneously in physical and in scale space has been anticipated by other authors. For instance Jimenez (1999), following the attached eddy concept of Townsend (1956), discusses an energy transfer diagram based on the assumed existence of a double structure for the turbulent field: the attached eddies with size comparable with their distance from the wall and a

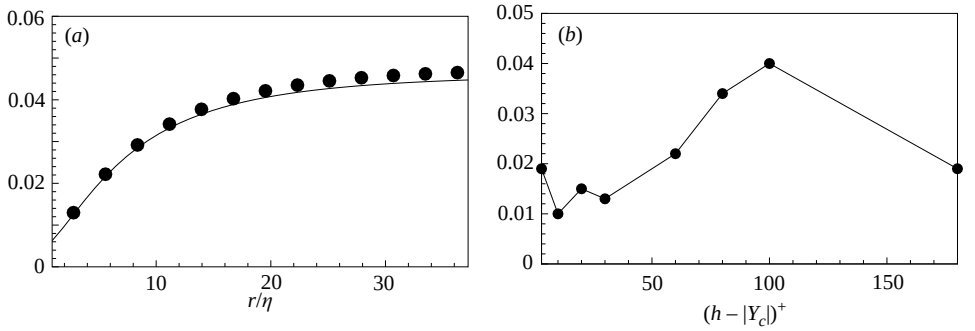

FIGURE 18. (*a*) *r*-averaged balance according to equation (4.10): ——, dissipation; ●, sum of all terms except dissipation for $Y_c^+ = 100$. (*b*) Residual of the *r*-averaged equation (4.10), normalized by the local dissipation, vs. distance from the wall.

background, incoherent turbulence. The attached eddies would be responsible for an inverse energy cascade from small eddies to larger ones, with the twofold effect of moving energy to larger scales and away from the wall. The generalized Kolmogorov equation used here offers a practicable way to measure the intensity of the different energy fluxes and provides, we believe, a complete and formally precise description of the detailed dynamics of turbulent fluctuations in the different regions of an inhomogeneous turbulent flow.

Appendix. Statistical convergence

When dealing with the statistical description of complex turbulent fields the issue of statistical convergence is always a crucial point. In the present case, the computational demand for well-converged statistics is partially mitigated by the stationarity of the field and by the homogeneity of the fluctuations with respect to translations in wall-parallel directions. The field is sampled at a number N of instants of time t_i and averages of a generic quantity q are defined as

$$\langle q(y) \rangle = \frac{1}{N} \sum_{i=1}^{N} \frac{1}{\Lambda_x \Lambda_z} \int_{-\Lambda_x/2}^{\Lambda_x/2} \int_{-\Lambda_z/2}^{\Lambda_z/2} q(x, y, z, t_i) \, \mathrm{d}x \, \mathrm{d}z. \tag{A 1}$$

An estimate on the convergence of the statistics can be obtained by considering the accuracy with which equation (4.10) is satisfied, see figure 18. From the numerical data-base, all contributions are found to sum-up to zero within a small statistical error $R_s(r, Y_c)$, whose magnitude is a measure of the statistical accuracy. As an example, figure 18(*a*) shows by symbols the sum of all terms in equation (4.10) except the contribution of the dissipation, which is separately displayed by the solid line. Their difference corresponds to $R_s(r, \bar{Y}_c)$ at location $\bar{Y}_c = 100$ where $|R_s|$ is largest. For each value of Y_c, the local maximum of R_s in r-space, typically attained at large separation, is plotted in figure 18(*b*) as a function of the distance from the wall. As shown, the overall statistical convergence is achieved within an accuracy better than 4% of the local dissipation.

Concerning the statistical significance of the results, the other relevant issue may concern the sensitivity to the dimensions of the computational domain. By comparing the results of our principal simulation ($\Lambda_x = 4$, $\Lambda_z = 2$) with those of a shorter run

with $\Lambda_x = 4\pi$, $\Lambda_z = 2\pi$ one can safely conclude that our main data set reproduces the appropriate dynamics in precise quantitative terms.

REFERENCES

Benzi, R., Amati, G., Casciola, C. M., Toschi, F. & Piva, R. 1999 Intermittency and scaling laws for wall bounded turbulence. *Phys. Fluids* **11**, 1–3.

Casciola, C. M., Benzi, R., Gualtieri, P., Jacob, B. & Piva, R. 2002 Double scaling in shear dominated flow. *Phys. Rev.* E **65**.

Casciola, C. M., Gualtieri, P., Benzi, R. & Piva, R. 2003 Scale by scale budget and similarity laws for shear turbulence. *J. Fluid Mech.* **476**, 105–114.

Danaila, L., Anselmet, F., Zhou, T. & Antonia, R. A. 2000 Turbulent energy scale budget equation in a fully developed channel flow. *J. Fluid Mech.* **430**, 87–109.

Eckelmann, U. 1974 The structure of the viscous sublayer and the adjacent wall region in a turbulent channel flow. *J. Fluid Mech.* **65**, 439–459.

Frisch, U. 1995 *Turbulence*. Cambridge University Press.

Gad-el-Hak, M. & Bandyopadhyay, P. R. 1994 Reynolds number effects in wall-bounded turbulent flows. *Appl. Mech. Rev.* **47**(8), 307–365.

Gualtieri, P., Casciola, C. M., Benzi, R., Amati, G. & Piva, R. 2002 Scaling laws and intermittency in homogeneous shear flow. *Phys. Fluids* **14**, 583–596.

Hinze, O. J. 1959 *Turbulence*. McGraw-Hill.

Hamilton, J. M., Kim, J. & Waleffe, F. 1995 Regeneration mechanisms of near-wall turbulence structures. *J. Fluid Mech.* **287**, 317–348.

Hill, R. J. 2002 Exact second-order structure-function relationships. *J. Fluid Mech.* **468**, 317–326.

Hill, R. J. & Borotav, N. 2001 Next order structure function equations. *Phys. Fluids* **13**, 276–283.

Jacob, B., Olivieri, A. & Casciola, C. M. 2002 Experimental assessment of a new form of scaling law for near wall turbulence. *Phys. Fluids* **14**, 481–491.

Jimenez, J. 1999 The physics of wall turbulence. *Physica* A **263**, 252–262.

Jimenez, J. & Moin, P. 1991 The minimal flow unit in near wall turbulence. *J. Fluid Mech.* **225**, 213–240.

Jimenez, J. & Pinelli, A. 1999 The autonomous cycle of near wall turbulence. *J. Fluid Mech.* **389**, 335–359.

Kim, J., Moin, P. & Moser, R. D. 1987 Turbulence statistics in fully developed channel flow at low Reynolds number. *J. Fluid Mech.* **177**, 133–166.

Klebanoff, P. S. 1954 Characteristics of turbulence in a boundary layer with zero pressure gradient. *NACA TN* 3178.

Kline, S. J., Reynolds, W. C., Schraub, F. A. & Runstadler, P. W. 1967 The structure of the turbulent boundary layers. *J. Fluid Mech.* **134**, 741–773.

Kolmogorov, A. N. 1941 The local structure of turbulence in incompressible viscous fluid for very large Reynolds number. *Dokl. Akad. SSSR* **30**, 301; reprinted in *Proc. R. Soc. Lond.* A **434**, 15–19, 1991.

Kurien, S. & Sreenivasan, R. 2001 Dynamical equations for high-order structure functions, and a comparison of a mean-field theory with experiments in three dimensional turbulence. *Phys. Rev.* E **64**, 056302.

Lindborg, E. 1999 Correction to the four-fifths law due to variations of the dissipation. *Phys. Fluids* **11**, 510–512.

Lundbladh, A., Henningson, D. S. & Johansson, A. V. 1992 An efficient spectral integration method for the solution of the time-dependent Navier–Stokes equations. *FFA-TN* 28. Aeronautical Research Institute of Sweden.

Monin, A. S. & Yaglom, A. N. 1975 *Statistical Fluid Mechanics*. MIT Press.

Moser, R. D., Kim, J. & Mansour, N. N. 1999 Direct numerical simulation of turbulent channel flow up to $\mathrm{Re}_\tau = 590$. *Phys. Fluids* **11**, 943–945.

Nikora, V. 1999 Origin of the "-1" spectral law in wall bounded turbulence. *Phys. Rev. Lett.* **83**, 734.

Oberlack, M. 2001 A unified approach for symmetries in plane parallel turbulent shear flows. *J. Fluid Mech.* **427**, 299–328.

Perry, A. E., Henbest, S. & Chong, M. S. 1986 A theoretical and experimental study of wall turbulence. *J. Fluid Mech.* **165**, 163–199.

Pope, S. B. 2000 *Turbulent Flows*. Cambridge University Press.

Robinson, S. K. 1991 Coherent motions in the turbulent boundary layer. *Annu. Rev. Fluid. Mech.* **23**, 601.

Ruiz-Chavarria, G., Ciliberto, S., Baudet, C. & Lévêque, E. 2000 Scaling properties of the streamwise component of velocity in a turbulent boundary layer. *Physica* D **141**, 183–198.

Saddoughi, S. V. & Veeravalli, S. G. 1994 Local isotropy in turbulent boundary layer at high Reynolds number. *J. Fluid Mech.* **268**, 333–372.

Toschi, F., Amati, G., Succi, S., Benzi, R. & Piva, R. 1999 Intermittency and structure functions in channel flow turbulence. *Phys. Rev. Lett.* **82**, 5044–5049.

Townsend, A. A. 1956 *The Structure of Turbulent Shear Flow*. Cambridge University Press.

Yakhot, V. 2001 Mean-field approximation and small parameter in turbulence theory. *Phys. Rev.* E **63**, 026307.

Zagarola, M. V. & Smits, A. J. 1997 Scaling of the mean velocity profile for turbulent pipe flow. *Phys. Rev. Lett.* **78**, 239–242.